Quantum Electronics **50** (7) 667–674 (2020)

https://doi.org/10.1070/QEL17295

High-speed implementation of holographic and diffraction elements using digital micromirror devices

N.N. Evtikhiev, E.Yu. Zlokazov, V.V. Krasnov, V.G. Rodin, R.S. Starikov, P.A. Cheremkhin

Abstract. **We report the results of simulations and experiments on the formation of light distributions by holograms and diffraction elements displayed by digital micromirror devices. Examples of successful experiments on the implementation of optical-digital systems based on them are demonstrated.**

Keywords: *digital micromirror device, hologram, diffractive optical element, correlator, invariant correlation filter, optical encryption, spatially incoherent illumination.*

1. Introduction

A digital micromirror device (DMD) is a microelectromechanical device that allows binary amplitude modulation of light [1]. Currently, DMDs are widespread and technologically advanced devices that have the highest operation speed among the available means of spatial light modulation. The best serial DMD models provide kilohertz frame rates at a resolution of a few megapixels and micron pixel size. High speed and spatial frequency characteristics of DMDs determine the interest to using them in diffractive optical-digital systems for various purposes [2] that require the formation of specified light distributions and/or spatial filtering.

This paper presents the results of experiments on the implementation of diffraction and holographic elements by means of the DMD intended for use in diffraction systems under both coherent and spatially incoherent illumination.

2. Digital micromirror devices

Modulation by DMDs is caused by the reflection of light from an array of micromirrors, on a silicon chip. Depending on the control signal, tiltable micromirrors of the DMD reflect incident radiation in two directions at angles of about ±15°. One of the directions corresponds to the state of a bright pixel, and the other to a dark one. DMDs provide binary amplitude modulation of light at a resolution of several megapixels, a frame rate of tens of kilohertz and a pixel size of about 10 μm. Such modulation parameters determine the possibility of creating relatively compact optical-digital diffraction DMD-based information processing systems that provide an input transmission capacity of several tens of Gbit per second. Of special interest is the use of DMDs for fast input into the optical system the diffraction elements that determine the system functionality. A significant problem in this case is the binary nature of the amplitude modulation produced by the DMD, which makes it necessary to use different (depending on the system type and purpose) approaches to ensure the required parameters of diffraction elements.

In order to determine the practical possibilities of using DMD in optical-digital diffraction systems, experiments were carried out to implement holographic and diffraction elements, including:

– computer-generated and digital holograms that form object images (Section 3);

– computer-generated Fourier holograms (CGFHs) and diffraction elements forming responses that correspond to correlation filters (Sections 4, 5);

– computer-generated Fourier holograms forming a coding response in an optical encryption system (Section 6);

– computer-generated diffraction elements without spatial carrier frequency, forming images of objects (section 7); and

– digital holograms forming images of objects (Section 8).

During the experiments, holographic and diffraction elements were implemented using serial Texas Instruments 0.7 XGA DLP7000 (resolution 1024×768 pixels, pixel size 10.8×10.8 μm, frame rate above 32 kHz) and Texas Instruments Discovery DLP9500BFLN DMDs (resolution 1920×1080 pixels, pixel size 10.8×10.8 μm, frame rate above 23 kHz). Their photos are presented in Fig. 1.

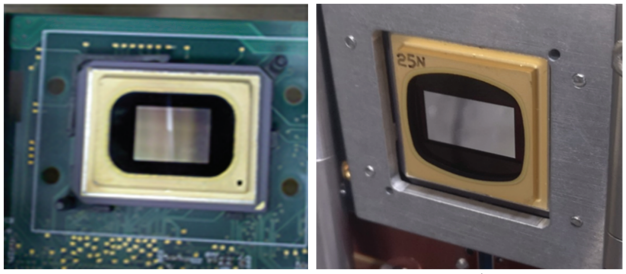

a b

Figure 1. DMDs: (a) Texas Instruments, model 0.7 XGA DLP7000, resolution 1024 × 768 pixels, frame rate above 32 kHz; (b) Texas Instruments, Discovery model on DLP9500BFLN chip, resolution 1920 × 1080 pixels, frame rate above 23 kHz.

N.N. Evtikhiev, E.Yu. Zlokazov, V.V. Krasnov, V.G. Rodin, R.S. Starikov, P.A. Cheremkhin National Research Nuclear University MEPhI, Kashirskoe shosse 31, 115409 Moscow, Russia;
e-mail: vitaly.krasnov@mail.ru

Received 18 February 2020; revision received 12 March 2020
Kvantovaya Elektronika **50** (7) 667–674 (2020)
Translated by V.L. Derbov

3. Implementation of computer-generated Fourier holograms

Currently, methods for computer-aided synthesis of holograms have received significant development [3–5]. For a given 2D distribution h, an off-axis computer-generated Fourier hologram can be obtained in the standard way using the formula

$$H_{\text{holo}}(x,y) = \text{Re}[H'(x,y)] - \min\{\text{Re}[H'(x,y)]\},$$

where

$$H'(x,y) = H(x,y)\exp[-\text{i}2\pi(\Delta_x x + \Delta_y y)];$$

$H(x,y)$ is the Fourier transform of the matrix h; and Δ_x and Δ_y are the displacements of the image h from the optical axis. Image reconstruction can be performed numerically by calculating the Fourier transform of the function of the hologram $H_{\text{holo}}(x,y)$, as well as optically in a coherent Fourier cascade scheme. Figure 2 shows the results of computer synthesis of Fourier holograms and numerical reconstruction of a greyscale image using them. The hologram is a greyscale raster image with a greyscale depth of 8 bits (levels from 0 to 255).

Figure 2. Computer-generated Fourier hologram for greyscale image: (a) central part of the hologram and (b) numerically reconstructed image (hereinafter, the first diffraction order).

The results of studying the capabilities of computer-generated Fourier holograms for reconstructing images and synthesising light beams with a given distribution of a complex amplitude demonstrate that when implemented using purely amplitude modulating means, the signal-to-noise ratio for the reconstructed signal is determined by the dynamic range of the carrier modulation producing the synthesised hologram [6]. When such a hologram is formed using a DMD, it is binarised, and the consequent reduction in the quality of the reconstructed light distribution relative to the initial one should be made minimal. In this case, it is necessary to separate two fundamental possibilities: the use of binary rasterisation for representing gradations of pixels and the use of direct binarisation of pixels [7–9].

In binary rasterisation, each pixel of the initial hologram is represented by several binary DMD subpixels, and so to represent $m^2 + 1$ sampling gradations of an $N \times N$ hologram, an $mN \times mN$ DMD is required. Direct binarisation methods are 'more economical' from the point of view the DMD size, since in this case, to output an $N \times N$ hologram, a DMD of the same size is required. However, limiting the number of the hologram quantisation levels to 2 leads to an increase in the quantisation noise in the signal generated by the hologram. To reduce the effect of quantisation noise on the output signal, various binarisation methods can be used, such as the global threshold methods (e.g., the Otsu method [10]) that use a single threshold value for the entire image, and the adaptive binarisation methods, in which the threshold is calculated for each image pixel based on statistical characteristics of the neighbouring pixels brightness [11, 12]. The choice of the binarisation method is determined in each case by the properties of the object and the conditions for using the synthesised hologram. Figure 3 illustrates the work of some binarisation methods.

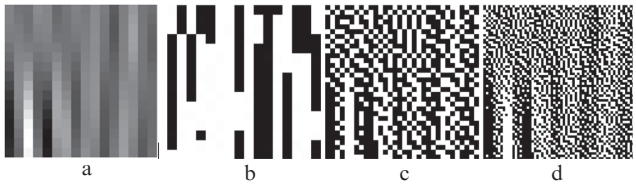

Figure 3. (a) Fragment of the original hologram, the same fragment (b) binarised by the Otsu method and (c, d) represented by random rasters with (c) five and (d) 17 gradations.

Figure 4 shows the results of binarisation of the Fourier hologram shown in Fig. 2 and the numerical reconstruction of an image from it. For binarisation the adaptive Bradley method [12] was used. It should be noted that the binary representation of holograms always reduces the quality of the reconstructed distributions relative to the initial ones (Fig. 4b), but in this regard, it is worth mentioning the possibilities of using widely known and actively developing methods for improving the quality of image reconstruction from Fourier holograms. One of these methods is multiplexing, applicable for any objects [13]; a multiplexed hologram is a set of identical holograms arranged symmetrically [14]. This approach allows getting the best-quality hologram image reconstruction. For holograms of purely amplitude objects, the efficiency can be improved by adding a random phase shift for each pixel [15]. Worth of particular consideration is the prob-

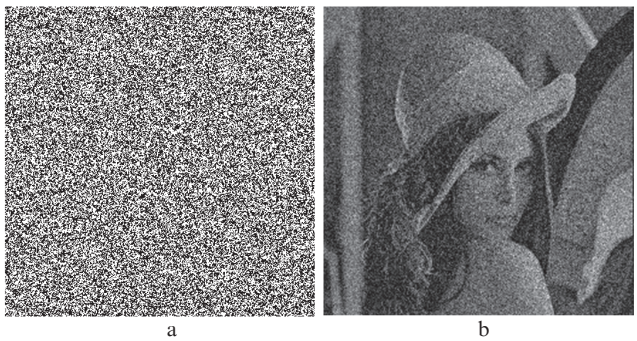

Figure 4. (a) Hologram binarised by the Bradley method shown in Fig. 2a, and (b) result of numerical reconstruction of the image of a greyscale object from it.

lem associated with the presence of phase distortions due to the non-flatness of the matrix and the protective glass of the DMD [16], but to the more advanced models of the DMDs this drawback is less inherent.

Figure 5 schematically shows an experimental setup for image reconstruction with Fourier holograms realised by means of DMDs. A plane-wave laser beam form the collimator consisting of a microlens L1, a micro aperture, and lens L2 illuminates the surface of the DMD. An image corresponding to a computer-generated hologram is displayed on the DMD. The modulated beam reflected by the DMD is directed to lens L3, in the rear focal plane of which the original image reconstructed in diffraction orders can be observed.

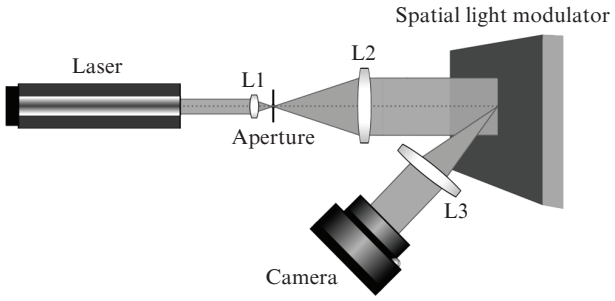

Figure 5. Experimental setup for reconstructing images from Fourier holograms.

Figure 6 shows the result of an experiment on the optical reconstruction of a greyscale image of a binarised computer-generated Fourier hologram. Despite the significant noise level, the image reconstructed by the hologram is of satisfactory quality, the elements of the displayed object can be easily extracted using known image processing tools.

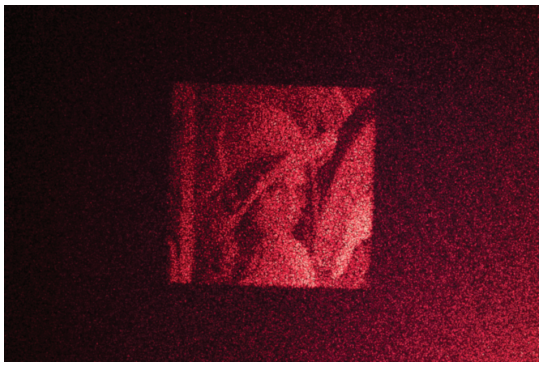

Figure 6. (Colour online) Result of the optical reconstruction of the image from the synthesised hologram shown in Fig. 4a.

4. Implementation of invariant correlation filters

The main advantage of the implementation of the correlation method of image recognition based on invariant optical-digital diffraction correlators is the high processing speed and energy efficiency of the calculations, achieved primarily by using DMDs. From the moment the idea of an optical correlator came to the latest impressive successes in this field, the main requirements are for the speed and resolution of the DMD used to load the input scene and the reference function [17–26]. Thus, a coherent correlator based on modern DMDs can have up to several million parallel channels with a switching rate of tens of kilohertz, which provides equivalent operation speed of the order of 10^{12}–10^{14} operations s^{-1} (operations per second), its power consumption being ~10 W. The corresponding energy efficiency will exceed 10^{11} operations s^{-1} W^{-1}. For comparison, supercomputers from the top of the Green500 list have a computational efficiency of no more than 1.7×10^{10} operations s^{-1} W^{-1}.

The work of an optical correlator is based on solving the problem of generating the impulse response of the optical system corresponding to the reference object, both for systems with a filter in the frequency plane and for systems with joint spectrum registration. At present, instead of the classical approach, which consists in implementing a matched filter with a high sensitivity to distortions, various types of invariant filters are used that are synthesised based on a set of reference images subjected to an *a priori* known type of distortion [17]. As a rule, an invariant filter is a complex-valued object. To form the corresponding complex impulse response of the optical system of the correlator in practice, methods should be used that take into account the characteristics of the DMD used. In this section of the paper, invariant filters are considered for coherent correlator schemes with filtering in the frequency plane (4*f* configuration), which, however, does not exclude the possibility of generalising the results, including for schemes with registration of a joint spectrum or for various versions of incoherent schemes. The experimental implementation of one of the incoherent schemes is presented in Section 5.

An effective way to obtain an invariant filter is computer synthesis of the corresponding holographic filter (HF), viz., the Fourier hologram of the original invariant filter, used, like the Van der Lugt filter, as a spatial frequency filter. The synthesis of HFs is similar to the synthesis of Fourier holograms considered in Section 2, and in the same way, to display a HF to a binary DMD, it is necessary to use binarisation methods [8, 9, 27–31]. Due to the resulting limitations on the dimensionality of processed images, the use of binary screening in the synthesis of an invariant filter, as a rule, is not efficient for improving the quality of recognition in the optical-digital correlator. Using multiplexing is almost impossible or complicates the scheme, and since the invariant filter is a complex-valued object, one cannot use the random phase mask method in the synthesis of HF. Nevertheless, in some cases it is possible to select the direct binarisation method, which provides the best result for this type of filter; in particular, in [8, 9], when recognising contour images, a significant improvement in the quality of recognition was demonstrated in comparison with the initial filter for HF binarisation by the global Otsu threshold method. Figure 7 shows an example of an invariant filter with a maximum height of the correlation peak [32], as well as the results of its numerical and optical reconstruction from the corresponding Fourier hologram binarised by the Bradley method.

Another way to implement invariant filters is based on the idea of adapting the filter to the modulation characteristic of the DMD and consists in searching for the so-called optimal projection of the Fourier transform of the filter on the values

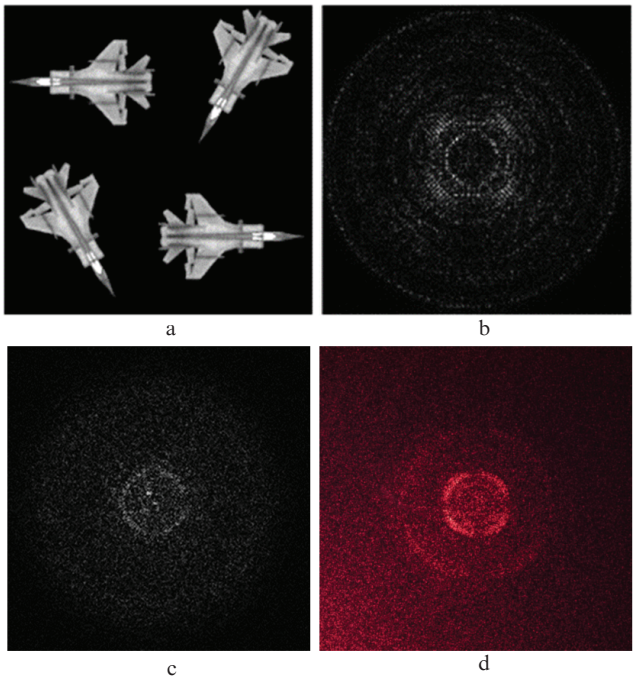

Figure 7. (Colour online) (a) Images of the object for which the correlation filter (CF) was synthesised; (b) amplitude distribution of the CF with the maximum height of the correlation peak, ensuring recognition invariance when turning in the plane of the object; (c) result of the HF numerical reconstruction; (d) result of the optical reconstruction of the HF using the DMD.

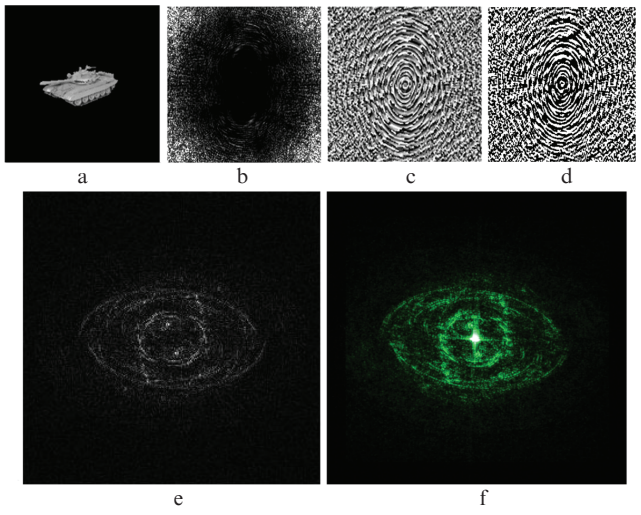

Figure 8. (Colour online) (a) Object for which CF is synthesised, (b, c) distributions of (b) amplitude and (c) phase of the Fourier transform of the CF with a minimum of noise and average correlation energy, (d) distribution of the binary amplitude of the optimal projection on the modulation characteristic of the DMD, and (e, f) response of the optimal projection, corresponding to the initial CF [(e) experiment and (f) calculation].

available for modulating DMD. In this case, the minimum Euclidean distance from the filter to its projection, as well as the estimation of the recognition error, can serve as a criterion of optimality. The optimisation parameters are the phase and amplitude factors common to all filter [ixels, which respectively rotate or scale the position of the values of the pixels of the Fourier transform of the filter on the modulation diagram. The problem of overlapping correlation and convolution regions arising with this approach is solved by introducing additional phase factors at the stage of obtaining the projection, which form the spatial carrier.

Figure 8 shows an example of the implementation of an optimal filter projection with a minimum of noise and correlation energy [33, 34] using a DMD. Euclidean distance optimisation is performed using the gradient descent method; the filter provides recognition invariance during spatial rotation of the object in the range of 180°. Despite the fact that such a method does not guarantee an exact correspondence of the amplitude and phase of the optical system to the amplitude and phase of the initial filter, in some cases the projection of the filter provides better recognition characteristics than the original filter [34].

5. Experimental implementation of the optical correlator based on the DMD in incoherent light

The combination of the characteristics of the DMD provides grounds to believe that modern DMDs can be successfully used as devices for the operational display of hologram filters in optical correlator setups not only under coherent illumination.

The optical correlator with the of filters displayed on the DMD [35, 36], used in the work for the operative recognition of objects, was constructed according to the scheme with only one lens to form the correlation distribution. The use of such a scheme is especially advisable when recognising objects in spatially incoherent light. In the output plane of the correlator, a correlation signal is formed in intensity rather than in amplitude, as in a coherent correlator, which eliminates phase distortions that affect the quality of the correlation signal.

The experimental setup is schematically shown in Fig. 9. Coherent radiation from a source (*1*) passes through a collimating system (microlens *2*, aperture, and lens *4*), in which a rotating ground glass (*3*) is used to destroy the spatial coherence of radiation. A transparency (*5*) with the image of the test object located in the input plane of the correlator is illuminated by spatially incoherent radiation, which is then reflected from a DMD (*6*) (Texas Instruments 0.7 XGA DLP7000) with the displayed holographic filter, synthesised on it in advance for the necessary reference object. A camera (*8*) is located in the output plane of the correlator to register

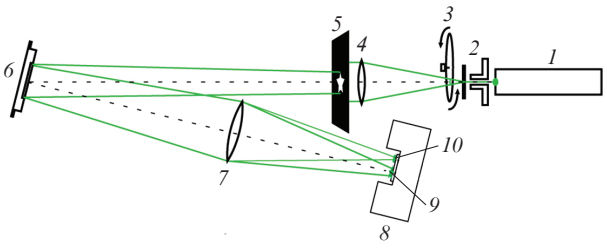

Figure 9. Schematic of the experimental incoherent holographic correlator setup based on the DMD: (*1*) laser; (*2*) microlens with a diaphragm; (*3*) rotating ground glass; (*4*) collimating lens; (*5*) transparency with an object to be recognised; (*6*) DMD with a holographic filter displayed on it; (*7*) lens; (*8*) recording camera; (*9*) zeroth diffraction order (image of the object); (*10*) first diffraction order (region of the correlation signal).

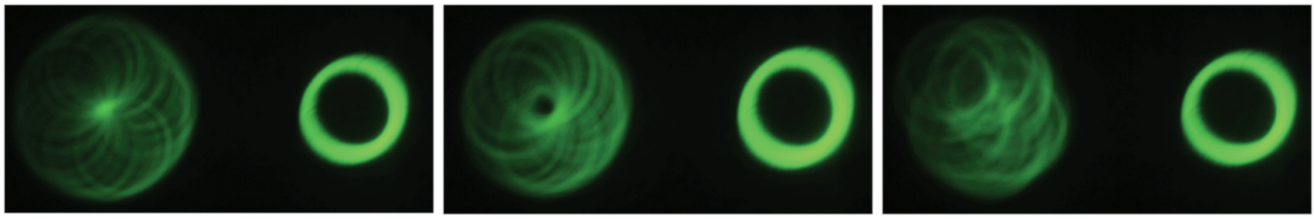

Figure 10. (Colour online) Images of signals at the correlator output (a) when the input and reference objects coincide, (b) when the scale of the objects does not match (the reference object is larger than the input one) and (c) when the objects are different (the reference object is the fish contour).

the structure formed by a lens (*7*), including the zeroth order (*9*) (image of the object) and the first diffraction order (*10*) (region of the correlation signal). From the presence of a localised intense peak in the first diffraction order, it can be concluded that the spatial characteristics of the reference and recognised objects coincide.

As test recognised objects, various contour images were used. Figure 10 shows the recognition results in the case when the input object remained unchanged, and hologram filters synthesised for various objects were sequentially displayed on the modulator. When the shapes of the input and reference objects coincide, a recognition signal is observed (Fig. 10a). If the scale of the objects (the reference object is larger than the input) and the shapes of the objects (the reference object is the contour of a fish) do not coincide, there are no localised correlation peaks (Figs 10b and 10c, respectively). Thus, the operation of incoherent correlator was demonstrated in the case of dynamically changing recognition parameters. The use of a DMD in such system provides the ability to perform tens of thousands of correlation comparisons per second.

6. Optical encryption of information using the DMD

The prospects of optical encryption methods [37–46] are due to the high security level provided by the 2D encryption keys combined with the high operation speed of optical methods. Since the creation of a high-speed encryption system requires the use of the fastest input devices, the use of DMDs in this case is preferable.

The experimental setup for optical encryption with spatially incoherent illumination based on two DMDs is shown in Fig. 11.

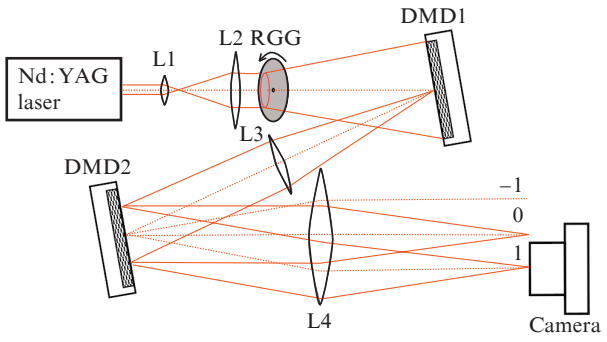

Figure 11. Schematic of the experimental setup for optical encryption with spatially incoherent illumination based on two DMDs.

A 200 mW Nd:YAG laser with a radiation wavelength of 532 nm was used as a source of monochromatic illumination. Spatial coherence was destroyed by a rotating ground glass (RGG). The encryption scheme was based on the classical 4*f* architecture. DMD1, used for information input, was in the front focal plane of the lens L3. DMD2, which served to output the synthesised holograms forming the encryption response of the system, was located in the rear focal plane of the lens L3 and in the front focal plane of the lens L4. Two Texas Instruments 0.7XGA DLP7000 DMDs had 1024×768 pixels (pixel size 10.8×10.8 μm). The Canon EOS 400D camera with a matrix of 3888×2592 pixels (pixel size 5.7×5.7 μm) was located in the rear focal plane of the lens L4 and recorded encoded images, which were an optical convolution of the image displayed on DMD1, with the response of the encoding hologram displayed by DMD2.

The encoded binary image displayed on the DMD1 is shown in Fig. 12a. A coding computer-generated binarised amplitude Fourier hologram containing 300×300 pixels and displayed on the DMD2 is shown in Fig. 12b. Figure 12c shows the response of the hologram in the first diffraction

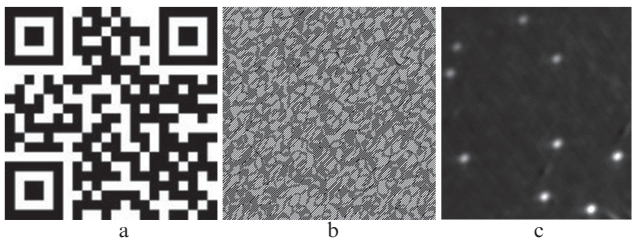

Figure 12. (a) Encoded binary image, (b) encoding amplitude Fourier hologram and (c) its response in the first diffraction order.

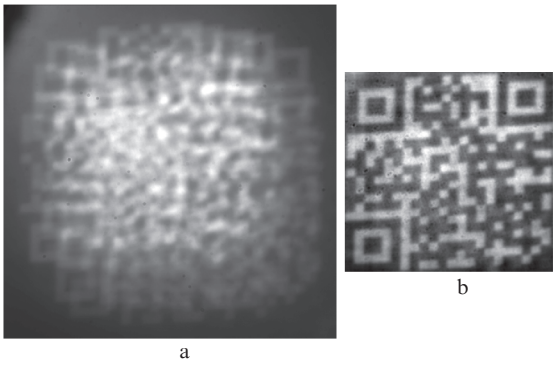

Figure 13. (a) Coded and (b) decoded images.

order. The coded image is shown in Fig. 13a. Decoding was carried out numerically by the inverse filtering method with Tikhonov regularisation [47]. The decoded image is shown in Fig. 13b. The visual quality of the decoded image is sufficiently high; the normalised standard deviation from the original is 0.18.

Thus, the possibility of a high-speed encryption system based on DMDs was experimentally demonstrated.

7. A binary amplitude diffraction element without spatial carrier frequency

The main disadvantages of the DMDs as compared to liquid crystal spatial light modulators (SLMs) are the impossibility of modulating the light phase and the binary nature of the modulation. In fact, the only diffractive optical element (DOE) suitable for the display on the DMD is a binary amplitude hologram. The disadvantages of such holograms include low diffraction efficiency of the order of 2%–4%, as well as the presence of undesirable diffraction orders, which requires their spatial separation and, accordingly, reduces the useful area of the reconstruction field.

To eliminate these disadvantages, a method for the synthesis of self-focusing amplitude DOEs without a spatial carrier frequency was proposed and tested. Such a DOE when illuminated by a spherical diverging wave of a certain radius of curvature at a given distance forms the required light distribution. The DOE synthesis method is based on an iterative algorithm similar to the Gerchberg–Saxton algorithm [48], with the differences that the synthesised DOE is amplitude rather than phase, and the incident wave front is diverging spherical. An example of a synthesised binary DOE without a carrier spatial frequency is shown in Fig. 14a, and its reconstruction field is shown in Fig. 14b. The DOE size was 1024×1024 pixels, the synthesis error was 7%, and the diffraction efficiency was 8%. The result of optical reconstruction of DOEs using a Texas Instruments Discovery DLP9500BFLN DMD is shown in Fig. 15.

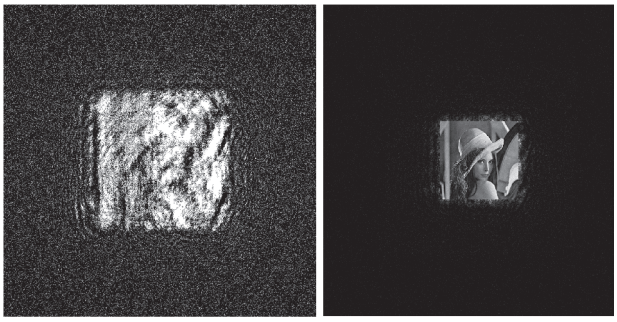

a b

Figure 14. (a) Synthesised DOE without the carrier spatial frequency and (b) its calculated response.

8. Use of DMD for optical reconstruction of scenes from digital holograms

At present, digital holography means the optical recording of the interference pattern from the object and reference waves by the digital matric registrar [49]. It is possible to reconstruct the image of an object from the obtained digital hologram numerically (using a computer) [50] and optically (when illuminating holograms displayed on SLMs) [51]. For most of the parameters, especially for frame speed, the DMD is a very preferable option for displaying holograms [2], which finds application in the problems of creating displays [52], in characterising light-scattering media [53], etc.

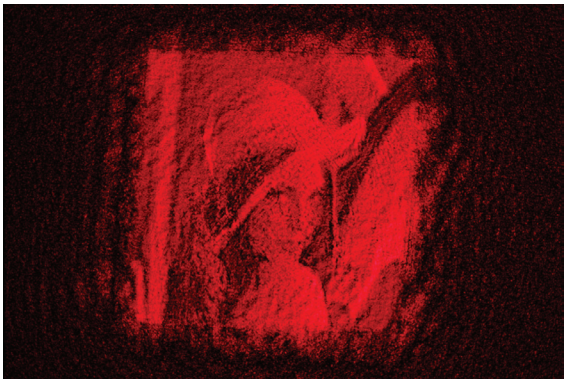

Figure 15. Result of the optical reconstruction of the DOE shown in Fig. 14a.

Since digital holograms are recorded by cameras, in which the brightness gradations are usually hundreds or thousands, then to display holograms on the DMD, one must first binarise the resulting image, as in the case of computer-generated holograms [8, 9]. When registering digital holograms of various objects, such binarisation methods are most applicable as introducing a local [7] or global threshold [7], using the standard [54, 55] or the point diffusion error operation [56], etc. In this case, it is necessary to take into account such parameter as the binarisation runtime. While the processing of a digital hologram with a size of 2048×2048 pixels using global binarisation methods based on the analysis of histograms takes milliseconds on a standard computer, some cluster methods take ~10 s [52], which may require additional computing power, including CUDA-type software architectures [56], graphic processors [56], programmable circuits [57], etc. All this leads to the need to find a compromise between the quality of the reconstructed images, diffraction efficiency, binarisation speed, and rate of hologram displaying on the DMD.

A fragment (128×128 pixels in size) of an optically registered digital Fresnel hologram of a diffuse object in its initial greyscale form and its numerically reconstructed image are shown in Fig. 16. A fragment of a hologram of the same size binarised by the Niblack method [58] and its numerically reconstructed image are shown in Figs 17a and 17b. The optical implementation of the reconstruction of images from digital holograms was carried out on a setup whose scheme is similar to that shown in Fig. 5; however, the image was recorded in the Fresnel diffraction zone. An example of image optically reconstructed from a binarised hologram displayed on the DMD is shown in Fig. 17c.

9. Conclusions

Thus, we present the results of simulations and optical experiments on the reconstruction of light distributions by holograms and diffraction elements realised using the DMDs, and demonstrate possible options for optical-digital systems

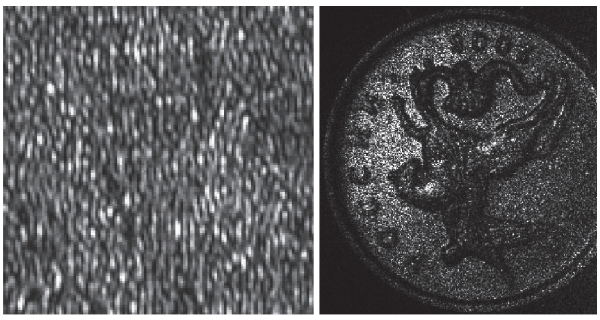

Figure 16. (a) Fragment of the recorded greyscale digital hologram and (b) image numerically reconstructed from it.

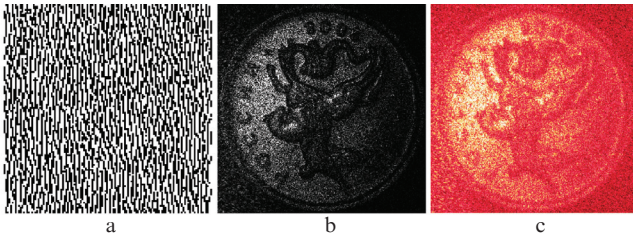

Figure 17. (a) Fragment of the binarised digital hologram and (b, c) images reconstructed from it (b) numerically and (c) optically.

based on them. As can be seen from the results of the experiments, the DMDs provide the reconstruction of the given light distributions with an acceptable quality comparable to the quality in numerical simulation. The main problem of using the DMDs in the construction of optical-digital systems is the negative effect of the binary representation of the holograms and diffraction elements on the quality of the reconstructed light distributions. However, in a significant number of cases, the binary character of the modulation in the DMDs can be taken into account and to some extent compensated in the synthesis of holograms and diffraction elements. The main advantages of the DMD, namely, high speed and spatial resolution, currently provide the possibility of implementing optical-digital systems for various purposes, with a transmission capacity of tens of gigabits per second.

Acknowledgements. This work was partially supported by the Russian Science Foundation (Section 6) (Grant No. 17-07-00829).

References

1. Hainich R.R., Bimber O. *Displays: Fundamentals and Applications* (Boca Raton, FL: CRC Press, 2016).
2. Kompanets I.N., Andreev A.L. *Quantum Electron.*, **47**, 294 (2017) [*Kvantovaya Elektron.*, **47**, 294 (2017)].
3. Shimobaba T., Ito T. *Computer Holography: Acceleration Algorithms and Hardware Implementations* (Boca Raton, FL: CRC Press, 2019).
4. Tsang P.W.M., Poon T.C., Wu Y.M. *Photon. Res.*, **6**, 837 (2018).
5. Kakue T., Wagatsuma Y., Yamada S., Nishitsuji T., Endo Y., Nagahama Y., Hirayama R., Shimobaba T., Ito T. *Opt. Eng.*, **57**, 061621 (2018).
6. Zlokazov E.Yu. *Jpn. J. Appl. Phys.*, **58**, SKKD04 (2019).
7. Cheremkhin P.A., Kurbatova E.A. *Opt. Lasers Eng.*, **115**, 119 (2019).
8. Starikov R.S., Zlokazov E.Yu., Shaulskiy D.V. *Proc. SPIE*, **7358**, 73580W (2009).
9. Evtikhiev N.N., Starikov S.N., Shaulskiy D.V., Starikov R.S., Zlokazov E.Yu. *Opt. Eng.*, **50**, 065803 (2011).
10. Otsu N. *IEEE Trans. Syst., Man, Cybern.*, **9** (1), 62 (1979).
11. Trier O.D., Taxt T. *IEEE Trans. Pattern Anal. Machine Intel.*, **17** (3), 312 (1995).
12. Bradley D., Roth G. *J. Graph. Tools*, **12**, 13 (2007).
13. Cheremkhin P.A., Evtikhiev N.N., Krasnov V.V., Porshneva L.A., Rodin V.G., Starikov S.N. *Proc. SPIE*, **9249**, 92491B (2014).
14. Christmas J., Collings N. *Appl. Sci.*, **8**, 685 (2018).
15. Burckhardt C.B. *Appl. Opt.*, **9** (3), 695 (1970).
16. Molodtsov D.Yu., Rodin V.G., Starikov S.N. *Phys. Proced.*, **73**, 338 (2015).
17. Vijaya Kumar B.V.K., Mahalanobis A., Juday R.D. *Correlation Pattern Recognition* (Cambridge, UK: Cambridge University Press, 2005).
18. Lugt A.V. *IEEE Transact. Inform. Theory*, **10**, 139 (1964).
19. Rau J.E. *J. Opt. Soc. Am.*, **56**, 1490 (1966).
20. Weaver C.S., Goodman J.W. *Appl. Opt.*, **5**, 1248 (1966).
21. Chao T.-H., Lu T., Walker B.P., Reyes G.F. *Proc. SPIE*, **9094**, 909402 (2014).
22. Evtikhiev N.N., Starikov S.N., Protsenko E.D., Zlokazov E.Yu., Solyakin I.V., Starikov R.S., Shapkarina E.A., Shaulskiy D.V. *Quantum Electron.*, **42**, 1039 (2012) [*Kvantovaya Elektron.*, **42**, 1039 (2012)].
23. Xu P., Hong C., Cheng G., Zhou L., Sun Z. *Opt. Express*, **23**, 6773 (2015).
24. Monjur M.S., Tseng S., Fouda M.F., Shahriar S.M. *Appl. Opt.*, **56**, 2754 (2017).
25. Ikeda K., Suzuki H., Watanabe E. *Opt. Lett.*, **42**, 2603 (2017).
26. Jridi M., Napoléon T., Alfalou A. *Appl. Opt.*, **57**, 2087 (2018).
27. Evtikhiev N.N., Starikov S.N., Sirotkin S.A., Starikov R.S., Zlokazov E.Yu. *Proc. SPIE*, **6977**, 69770C (2008).
28. Evtikhiev N.N., Starikov S.N., Zlokazov E.Yu., Sirotkin S.A., Starikov R.S. *Quantum Electron.*, **38**, 191 (2008) [*Kvantovaya Elektron.*, **38**, 191 (2008)].
29. Evtikhiev N.N., Starikov S.N., Starikov R.S., Zlokazov E.Y. *Proc. SPIE*, **7340**, 73400R (2009).
30. Evtikhiev N.N., Shaulskiy D.V., Zlokazov E.Y., Starikov R.S. *Proc. SPIE*, **8748**, 87480O (2013).
31. Shaulskiy D., Evtikhiev N., Starikov R., Starikov S., Zlokazov E. *Proc. SPIE*, **9094**, 90940K (2014).
32. Mahalanobis A., Vijaya Kumar B.V.K., Song S., Sims S.R.F., Epperson J.F. *Appl. Opt.*, **33**, 3751 (1994).
33. Ravichandran G., Casasent D. *Appl. Opt.*, **31**, 1823 (1992).
34. Shaulskiy D.V., Evtikhiev N.N., Zlokazov E.Y., Starikov S.N., Starikov R.S., Petrova E.K., Molodtsov D.Y. *Proc. SPIE*, **9598**, 95980T (2015).
35. Molodtsov D.Yu., Rodin V.G. *Proc. SPIE*, **10176**, 101761A (2016).
36. Rodin V.G. *Computer Optics*, **42** (3), 347 (2018) [*Komp'yuternaya Opt.*, **42** (3), 347 (2018)].
37. Refregier P., Javidi B. *Opt. Lett.*, **20**, 767 (1995).
38. Rajput S.K., Nishchal N.K. *Appl. Opt.*, **51**, 1446 (2012).
39. Markman A., Wang J., Javidi B. *Optica*, **1**, 332 (2014).
40. Situ G., Zhang J. *Opt. Lett.*, **29**, 1584 (2004).
41. Cheremkhin P.A., Krasnov V.V., Rodin V.G., Starikov R.S. *Laser Phys. Lett.*, **14,** 026202 (2017).
42. Krasnov V.V., Starikov S.N., Starikov R.S., Cheromkhin P.A. *Russ. Phys. J.*, **58**, 1394 (2016) [*Izv. Vyssch. Uchebn. Zaved., Ser. Fiz.*, **58**, 29 (2016)].
43. Tajahuerce E., Lancis J., Javidi B., Andrés P. *Opt. Lett.*, **26**, 678 (2001).
44. Barrera J.F., Mira A., Torroba R. *Opt. Express*, **21**, 5373 (2013).
45. Evtikhiev N.N., Krasnov V.V., Kuzmin I.D., Molodtsov D.Yu., Rodin V.G., Starikov R.S., Cheremkhin P.A. *Quantum Electron.*, **50**, 195 (2020) [*Kvantovaya Elektron.*, **50**, 195 (2020)].
46. Bondareva A.P., Cheremkhin P.A., Krasnov V.V., Rodin V.G., Starikov R.S., Starikov S.N. *Proc. SPIE*, **9648**, 96480S (2015).
47. Arsenin V.YA., Tikhonov A.N. *Metody resheniya nekorrektnykh zadach* (Methods for Solving Ill-Posed Problems) (Moscow: Nauka, 1979).
48. Gerchberg R.W., Saxton W.O. *Optik*, **2**, 237 (1969).

49. Schnars U., Falldorf C., Watson J., Jüptner W. *Digital Holography and Wavefront Sensing: Principles, Techniques and Applications* (Berlin, Heidelberg: Springer-Verlag, 2015).
50. Verrier N., Atlan M. *Appl. Opt*., **50**, H136 (2011).
51. Tsang P.W.M., Poon T.-C. *IEEE Transact. Industr. Inform*., **12**, 886 (2016).
52. Pan Y., Liu J., Li X., Wang Y. *IEEE Transact. Industr. Inform.*, **12**, 1599 (2016).
53. Conkey D.B., Caravaca-Aguirre A.M., Piestun R. *Opt. Express*, **20**, 1733 (2012).
54. Yang G., Jiao S., Liu J.-P., Lei T., Yuan X. *Appl. Opt*., **58**, 5547 (2019).
55. Cheremkhin P.A., Kurbatova E.A., in *Proceedings of Digital Holography and 3-D Imaging* (USA, 2019) Th3A.22.
56. Makey G., El-Daher M.S., Al-Shufi K. *Optik*, **124**, 5486 (2013).
57. Buckley E. *J. Display Technol*., **7**, 70 (2011).
58. Niblack W. *An Introduction to Digital Image Processing* (Upper Saddle River, NJ, USA: Prentice Hall, 1986).